JCTC Journal of Chemical Theory and Computation

Article

pubs.acs.org/JCTC

First and Second One-Electron Reduction of Lumiflavin in Water—A First Principles Molecular Dynamics Study

Murat Kılıç and Bernd Ensing*

Van't Hoff Institute for Molecular Sciences, University of Amsterdam, Science Park 904, 1098 XH, Amsterdam, The Netherlands

Supporting Information

ABSTRACT: Flavins are ubiquitously found in nature as cofactors in proteins that regulate electron and proton transfer reactions. The electron and proton affinities of flavins are modulated by their molecular environment. Using density functional theory based molecular dynamics simulations, we have studied the first and second reduction reactions of the prototypical flavin named lumiflavin in aqueous solution. We find that the reduction potential, calculated using free energy perturbation simulations, has the typical parabolic shape as predicted by Marcus' theory of electron transfer. The water solvent structure undergoes significant changes within the first coordination shell upon lumiflavin reduction. These structural changes account largely for the reorganization free energy term in the measured redox potential. However, in the second reduction reaction, from semiquinone to fully reduced lumiflavin, also the inner-sphere reorganization contributes significantly via the increased "butterfly" bending of the flavin. This butterfly bending causes a deviation from the linear response approximation that underlies Marcus' theory of electron transfer.

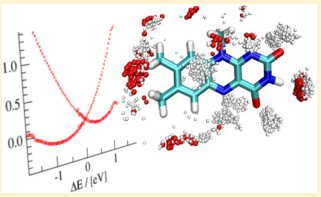

INTRODUCTION

Flavins are a group of chemical compounds that are biochemically derived from riboflavin, also known as vitamin B_2. They can accept up to two electrons and two protons and therefore play an important role in biochemical oxidation–reduction reactions. Enzymes that bind as a cofactor a flavin, such as flavin adenine dinucleotide (FAD) or flavin mononucleotide (FMN), are called flavoproteins and include hydroxylases, dehydrogenases, and oxidases. Apart from this already versatile ground-state redox biochemistry, flavins can also be photoreduced by the absorption of blue light and are therefore found as the chromophore in several photoreceptor families.

The reduction potential of the flavin is largely modulated by its molecular environment, and different flavoproteins can display therefore rather different redox and midpoint potentials.[1] For example, the one- and two-electron reduction potentials of several flavins were found to correlate with the "butterfly" bending of the flavin (isoalloxazine) ring system,[2] which could be induced by the enzyme's binding pocket as a mode of modulation. But also covalent bonding, hydrogen bonding, and electrostatic interactions between the flavin and the apoprotein can tune the redox properties.[3,4] The redox potential of flavins in various media has already been estimated in several experimental[5−8] and numerical[9−11] studies. However, a detailed molecular picture of the effect of the environment on the redox properties of flavins and the reorganization of the environment upon flavin reduction is still unclear.

Neutral flavin can undergo four sequential reduction and protonation steps,

$$LF + e^- \rightarrow LF^- \quad (1)$$

$$LF^- + H^+ \rightarrow LFH \quad (2)$$

$$LFH + e^- \rightarrow LFH^- \quad (3)$$

$$LFH^- + H^+ \rightarrow LFH_2 \quad (4)$$

Here, we study the one-electron reduction processes, steps 1 and 3, of lumiflavin in aqueous solution by ab initio (density functional theory) molecular dynamics simulations. Lumiflavin is the smallest member of the flavin family in which the side-chain of the isoalloxazine ring system is a methyl group (see Figure 1). Water is the typical solvent for electrochemical experiments. Due to the relatively high dipole moment and high mobility of the water molecules, the solvent environment has a considerable effect on the redox potential of lumiflavin. Although water provides an isotropic environment on the longer length scale, on the molecular scale the solvent structure

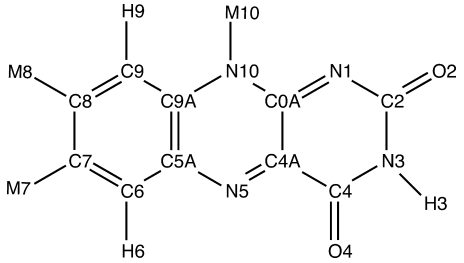

Figure 1. Structural motif and labeling of lumiflavin. In the biochemically important flavins, riboflavin, flavin mononucleotide, and flavin adenine dinucleotide, the M10 methyl group is replaced by different groups. The N1 and N5 nitrogen atoms are easily protonated in the reduced form of flavin.

Received: February 1, 2013
Published: July 30, 2013

and the solvent reorganization may be highly anisotropic due to the amphiphilic nature of the lumiflavin molecule.

To model the reduction of lumiflavin in water, we follow the approach that was pioneered by Warshel[12] and Warshel and King[13] and more recently further developed for density functional theory based simulations by Sprik and co-workers.[14−21] The latter authors have studied the redox properties of various aqueous transition metal ions such as the Ag^{2+}/Ag^{+} ions[14−16] and the Ru^{3+}/Ru^{2+} ions,[17,18] as well as some small organic compounds such as quinones,[19] tetrathiafulvalene, and thianthrene.[20] One striking observation of their work is that the water solvent does not always respond in a linear fashion to a change in the solute charge, for example, when the coordination number changes upon electron transfer, as is the case for the Ag^{2+}/Ag^{+} and Cu^{2+}/Cu^{+} reduction reactions.[14−16,22,23] This implies that Marcus classical theory of electron transfer, which assumes a linear response, does not hold in these cases. Anticipating our results on the lumiflavin reduction, here we find that the second reduction displays a significant nonlinearity.

In the following, we first briefly describe the background of Marcus' theory of electron transfer that underlies our calculations in the Methods section, followed by the computational details of our ab initio molecular dynamics simulations. The Results section describes first our calculations of lumiflavin in the gas phase; then we characterize the structure of the water solvent around lumiflavin in the different oxidation states, and finally we present our calculations of the first and second reduction processes of lumiflavin in water.

METHODS

Marcus theory of electron transfer explains the rate at which an electron can move from an electron donor to an electron acceptor in a polarizable medium.[24,25] Marcus theory assumes linear response of the environment polarization and, second, that the amount of polarization is described by the vertical energy gap, ΔE. Here, the vertical energy gap refers to the energy required to move the electron from donor to acceptor at fixed nuclear coordinates, that is, without relaxing the environment. As the actual jump of the electron is much faster than the reorganization of the environment nuclear coordinates, this (nonelectronic) environment polarization is the slow variable that governs the electron transfer process. Using ΔE as the reaction coordinate, Marcus' famous picture of the free energy landscape consists simply of two parabolic curves that describe the reactant and product states and that cross at the transition state. In this picture, the reaction free energy can be seen as the sum of the vertical energy gap and the reorganization free energy of the environment, λ. Note that the first step, ΔE, occurs at fixed geometry and thus does not contain an entropic contribution.

Modeling electron transfer using a self-consistent field electronic structure method such as density functional theory (DFT) is fraught with difficulty, because imposing the transfer of an electron is far from trivial and also the use of ΔE as a reaction coordinate is impractical. Sprik and co-workers circumvent the direct transfer by focusing on a redox half reaction, conventionally written in reduction form as

$$\mathrm{O} + \mathrm{e}^{-} \rightarrow \mathrm{R} \tag{5}$$

in which case the total DFT energies of the oxidant O and the reductant R can be computed separately in the electronic ground state and the energy of e^{-} is taken as the chemical potential of an electron in a bath of electrons. Although in principle this allows for the calculation of the redox potential for reaction 5, also here arise a number of complications. In the first place, components O and R have different charges and charge distributions that, in a setup with periodic boundary conditions, give different self-interaction energies, leading to a systematic, box-size dependent offset in the energy difference.[26,27] Second, the calculation does not account for the effects due to having an electrode in the solvent, which affects the reference potential and thus makes direct comparison to experimental redox potentials difficult. The approach is thus limited to computing relative redox potentials between similar redox reagents with the same solvent and the same box size.

Within this limitation however, Sprik and co-workers[14−18,20,21] showed that the approach of considering the half reactions is a very powerful means to compute redox potentials with ab initio DFT molecular dynamics (MD). Marcus theory also applies for half reaction eq 5, and moreover, the free energy curves can be obtained from the distribution of the vertical gap energies. Conforming with eq 5, the energy gap is defined as the energy needed to add an electron to the system:

$$\Delta E = E_{\mathrm{R}}(\mathbf{r}^{N}) - E_{\mathrm{O}}(\mathbf{r}^{N}) \tag{6}$$

The energy gap distributions in the oxidized and reduced states can be obtained by sampling over many configurations of the atomic positions with a DFT−MD simulation of the system in each state and computing the energy difference of the configurations with either an added or removed electron. For long enough sampling times, the histogram of ΔE approaches the ensemble average of the probability density

$$\begin{aligned} P_{\eta}(\Delta E') &= Z^{-1} \int \mathrm{d}\mathbf{r}^{N}\, \mathrm{e}^{-\beta E_{\eta}}\, \delta(\Delta E - \Delta E') \\ &= \lim_{\tau\to\infty} \frac{1}{\tau} \int_{0}^{\tau} \delta(\Delta E(\mathbf{r}^{N}(t)) - \Delta E')\, \mathrm{d}t \end{aligned} \tag{7}$$

in which $P_{\eta}(\Delta E')$ is the probability to find $\Delta E'$ in state η = O (oxidized) or η = R (reduced). Here, $\beta = 1/k_{\mathrm{B}}T$, with k_{B} being Boltzmann's constant and T the temperature. Z is the partition function, and $\mathbf{r}^{N}$ are the atom coordinates. The Landau free energy of the system as a function of the ΔE coordinate is then

$$A_{\eta}(\Delta E) = -k_{\mathrm{B}}T \ln[P_{\eta}(\Delta E)] \tag{8}$$

In the case that the $P_{\eta}(\Delta E)$ distributions are Gaussian, it follows that the free energy curves are parabolic. That the fluctuations in ΔE are Gaussian is one of the main assumptions in Marcus' theory of electron transfer, which has a number of interesting consequences that we briefly summarize next.

Let us consider a parabolic free energy curve for the oxidized state centered at the average energy gap, $\langle \Delta E \rangle_{\mathrm{O}}$:

$$A_{\mathrm{O}} = a(\Delta E - \langle \Delta E \rangle_{\mathrm{O}})^{2} \tag{9}$$

in which we choose the curve minimum as the zero of our free energy scale, and a sets the curvature of the parabola and is related to the reorganization free energy, λ, as we will see shortly. Since the variable on the x axis is the vertical energy gap between the free energy curves A_{O} and A_{R} (and we have adopted the reduction potential convention in eq 6), the free energy curve for the reduced state must equal

$$A_{\mathrm{R}}(\Delta E) = A_{\mathrm{O}}(\Delta E) + \Delta E \tag{10}$$

To find the minimum of the second curve, we insert eq 9 and solve $(dA_R)/(d\Delta E) = 0$, which gives

$$\langle \Delta E \rangle_R = \langle \Delta E \rangle_O - \frac{1}{2a} \tag{11}$$

Inserting eq 9 and eq 11 into eq 10 leads then to the expression of the second curve:

$$A_R = a(\Delta E - \langle \Delta E \rangle_R)^2 + \langle \Delta E \rangle_R + \frac{1}{4a} \tag{12}$$

Thus the free energy profile of the reduced state is also a parabola with the same curvature parameter a as the curve of the oxidized state, but vertically shifted by $\langle \Delta E \rangle_R + 1/(4a)$. This shift is the reaction free energy, or redox potential, which can be rewritten using eq 11 in the well-known form of

$$\Delta A = \frac{1}{2}(\langle \Delta E \rangle_R + \langle \Delta E \rangle_O) \tag{13}$$

The reorganization free energy, λ, can now be defined as $\lambda = \Delta A - \langle \Delta E \rangle_R$, which can be combined with eq 13 to give

$$\lambda = \frac{1}{2}(\langle \Delta E \rangle_O - \langle \Delta E \rangle_R) \tag{14}$$

By combining eq 14 with eq 11, we see that the parameter a is connected to the reorganization free energy by $a = (4\lambda)^{-1}$.

Finally, we can write for the probability to measure a certain ΔE:

$$P_\eta(\Delta E) = Z^{-1} \exp\left[-\frac{A_\eta(\Delta E)}{k_B T}\right] = Z^{-1} \exp\left[\frac{(\Delta E - \langle \Delta E \rangle_\eta)^2}{4\lambda k_B T}\right] \tag{15}$$

which is a Gaussian centered at $\langle \Delta E \rangle_\eta$ with variance $\sigma_\eta^2 = 2\lambda k_B T$ or

$$\lambda_\eta = \frac{\sigma_\eta^2}{2k_B T} \tag{16}$$

which again relates the reorganization free energy with the fluctuations in ΔE.

Equation 16 allows us to obtain an estimate of the reorganization free energy from a single simulation in the oxidized or reduced state and a measurement of the fluctuations σ^2 in ΔE. Comparing each of these numbers with that obtained using eq 14 allows us to assess the accuracy of our simulations or to test the validity of the linear response assumption underlying Marcus' theory. The same holds for a calculation of ΔA_η as

$$\Delta A_O = \langle \Delta E \rangle_O - \lambda_O$$

and

$$\Delta A_R = \langle \Delta E \rangle_R + \lambda_R \tag{17}$$

which for each also requires only sampling of a single oxidation state and can be compared to each other and to ΔA obtained with eq 13.

Summarizing, we see that the two parabolic curves that make up the well-known free energy landscape from Marcus' theory of electron transfer are defined by their minima at $\langle \Delta E \rangle_O$ and $\langle \Delta E \rangle_R$ and a curvature parameter a. The parameters are related by eq 12 (or eq 14 as $a = (4\lambda)^{-1}$) so that only two parameters have to be known to draw the free energy diagram. Consequently, the redox potential and the reorganization free energy can be obtained from the first and second moments of the vertical energy gap sampled in a single state (eq 16) or from the average energy gaps of both states (eq 13 and eq 14). The free energy curves can also be obtained as the logarithm of a histogram of the vertical energy gap (eq 8), which does not require the assumption of linear response theory and Gaussian fluctuations of ΔE.

COMPUTATIONAL SETUP

All electronic structure calculations and ab initio molecular dynamics simulations were performed using DFT with the Perdew–Burke–Ernzerhof (PBE)[28] exchange-correlation functionals as implemented in Quickstep,[29] which is part of the CP2K program (version 2.1.347).[30] The CP2K program is based on a hybrid Gaussian and plane wave scheme in which the wave functions are expanded using a Gaussian basis set, and an auxiliary basis of plane waves is employed to expand the density.[31] We used pseudopotentials of the Goedecker–Teter–Hutter (GTH) type, based on the parametrization of Hartwigsen–Goedecker–Hutter[32,33] and adapted for the density functional. A split valence Gaussian basis set designed specifically for these pseudopotentials of double-ζ quality and with polarization functions (DZVP[34]) was employed for all atoms including hydrogen. Tests with the larger TZVP basis set available in CP2K gave no significantly different results. The auxiliary plane wave basis expansion was cutoff at 280 Ry.

The calculations of the lumiflavin in the gas phase were performed in a cubic unit cell with an edge of 20 Å and subject to periodic boundary conditions. To isolate the unit cell from electrostatic interactions with periodic neighbors, we used the scheme of Martyna and Tuckerman.[35] Figure 2 shows the box size dependence of the vertical energy gap of lumiflavin in the gas phase, which shows convergence to within 1 kcal/mol beyond a length of 18 Å.

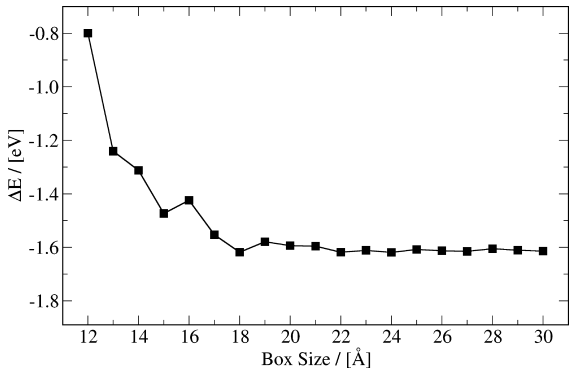

Figure 2. Vertical energy gap of lumiflavin in the gas phase as a function of the length of the cubic box edge.

The model of aqueous lumiflavin contained one lumiflavin molecule and 102 water molecules in a periodic cubic unit cell with an edge of 15.148 Å. The size of the cell was determined from a classical NPT simulation of the flavin in a cubic, 53 Å large box of water using the Gromos94 force field. The ab initio molecular dynamics simulations used the Born–Oppenheimer method with a time step of 0.5 fs in the canonical (NVT) ensemble. The CSVR (Canonical Sampling through Velocity Rescaling)[36] thermostat was used to maintain a constant

dx.doi.org/10.1021/ct400088g | J. Chem. Theory Comput. 2013, 9, 3889–3899

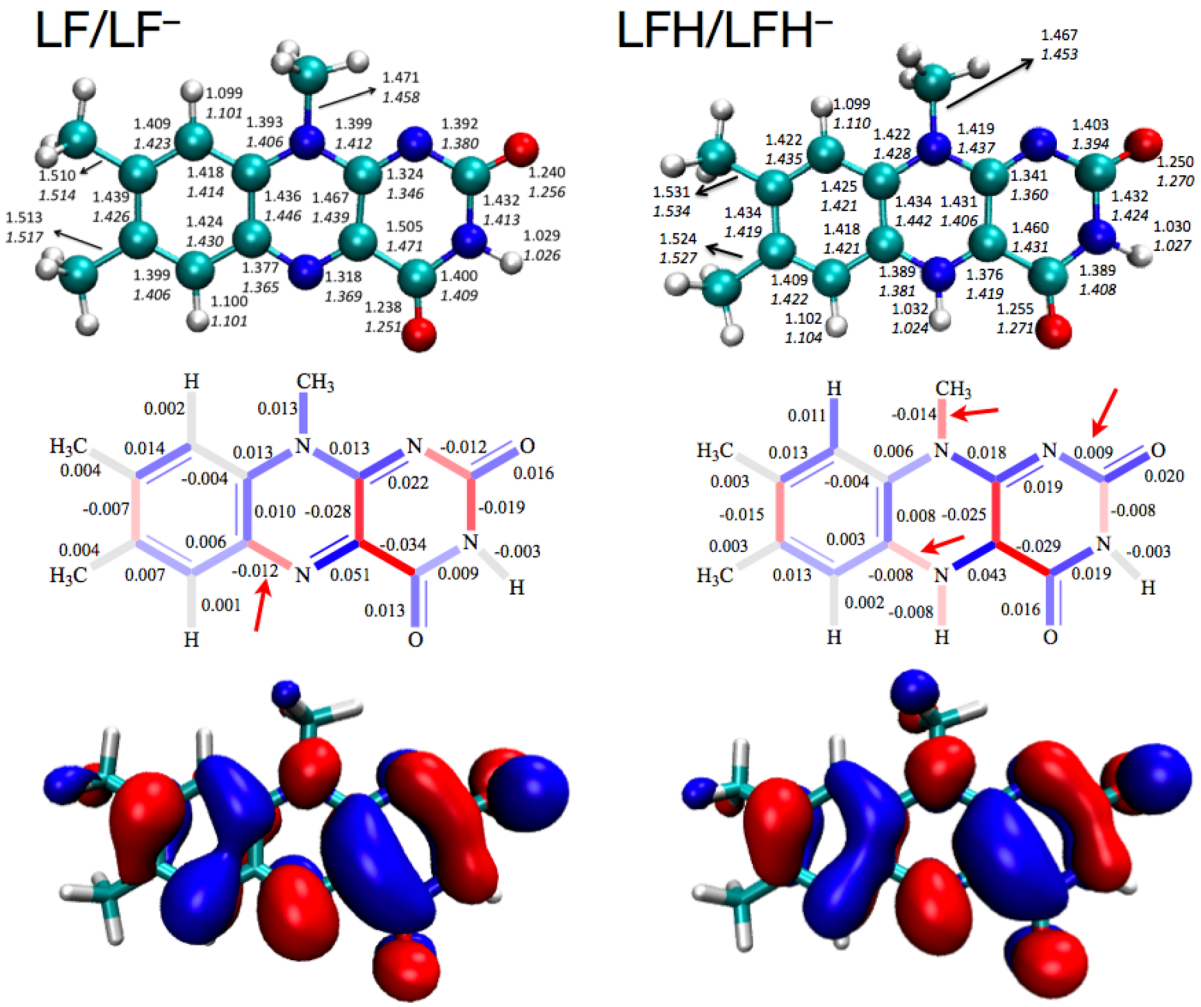

Figure 3. Top panels: bond lengths (Å) of the neutral (top number) and anionic (bottom italic number) lumiflavin at 0 Kelvin in a vacuum using DFT−PBE/DZVP. Middle panels: change in the molecular geometry upon addition of the electron to the neutral lumiflavin. The red to blue color coding highlights the shortening and elongation of bonds respectively. Bottom panel: LUMO of the neutral LF (left) and LFH (right). LUMO nonbonding (node) and bonding positions correlate with shortening and elongation of bonds. Exceptions to these correlations are denoted by a red arrow in the middle panels.

temperature. We performed AIMD simulations of neutral lumiflavin (LF); the singly reduced, anionic lumiflavin (LF^-); the neutral semiquinone state (LFH); and the doubly reduced lumiflavin (LFH^-). The simulations were performed at T = 300 K and at T = 350 K. It is known that AIMD simulations using current GGA functionals somewhat overstructure water solvent and underestimate the self-diffusion at T = 300 K. The simulation at T = 350 K is expected to give a closer representation of the behavior of the aqueous system at room temperature.[37] The systems were equilibrated for at least 25 ps, after which between 20 and 45 ps of simulation was performed for analysis. At each time step, we computed, in addition to the total energy of the system, also the total Kohn−Sham energy of the system with an extra electron (for the neutral systems) or with an electron less (for the anionic systems), to obtain the vertical energy gap ΔE. In CP2K, this can be done, for each state, with a single, so-called mixed Hamiltonian simulation, using

$$H_\eta = \eta H_R + (1 - \eta) H_O \quad (18)$$

With the coupling parameter η equal to zero, the Hamiltonian is that of the lumiflavin in the neutral oxidized state, whereas with η = 1, the Hamiltonian is that of the anionic reduced state. An intermediate value allows for simulation on a fictitious potential that is a superposition of the two redox states, which corresponds to a state with a fractional electron. The ΔE is obtained from the H_R and H_O energies, which are printed to output in addition to the H_η energy.

RESULTS

Lumiflavin in the Gas Phase. We start our investigation of lumiflavin with the molecule in the gas phase, that is without any molecular environment, by computing the T = 0 K minimum energy structure at the DFT−PBE level of theory using the DZVP basis set. The neutral lumiflavin molecule has a planar three-ring isoalloxazine structure, which is shown in ball−stick representation in Figure 3. Adding an electron to the neutral flavin without relaxing the structure lowers the total energy with ΔE_O = −1.60 eV. This is the zero-Kelvin vertical energy gap of the electron transfer for the half reaction

$$LF + e^- \rightarrow LF^- \quad (19)$$

Relaxation of the structure after adding the electron gives a further lowering of the total energy of −0.17 eV. This is the zero-Kelvin inner-sphere reorganization energy, which gives

dx.doi.org/10.1021/ct400088g | J. Chem. Theory Comput. 2013, 9, 3889−3899

Table 1. Zero Kelvin Gas-Phase Energies (eV) of the Vertical Energy Gap in the Neutral Oxidized State (ΔE_O) and in the Anionic Reduced State (ΔE_R)[a]

	PBE			M06-L[9]	B3LYP[9]
reduction reaction	ΔE_O	ΔE_R	ΔU	ΔU	ΔU
(1) LF + e^- → LF^-	−1.60	−1.92	−1.77	−1.78	−1.91
(2) LFH + e^- → LFH^-	−1.72	−2.00	−1.83	−1.95	−2.12

[a] ΔU is the energy difference between the geometry optimized states. The last two columns show the ΔU results from ref 9 using the M06-L and B3LYP density functionals.

together with the vertical energy gap a total electron affinity for lumiflavin of $\Delta U = -1.77$ eV. Similar values are found for the second reduction of the (hydrated) semiquinone molecule, as compiled in Table 1. The last columns show the results of Bhattacharyya et al. computed with the M06-L and B3LYP density functionals.[9] Especially for the second reduction reaction, the ΔU value found with PBE is somewhat less negative than that obtained with the M06-L and B3LYP functionals. The difference between the electron affinities of LF and LFH of 0.06 eV using the PBE functional is therefore smaller than that using M06-L (0.17 eV) or B3LYP (0.22 eV). An underestimation of this electron affinity difference using PBE will lead to an overestimation of the semiquinone (LF^-/LFH) formation constant, as we will see later on. The bond distances of the neutral and anionic lumiflavin are indicated in Figure 3. The red-to-blue color coding in the figure (middle panel) underlines the changes in bond lengths upon electron addition, with bright red indicating the most shortened bonds and bright blue indicating the most elongated bonds.

Qualitatively, these small changes in the structure (or "inner sphere reorganization") can be understood from the change in the electronic structure of the molecule. In particular, it is interesting to compare the structure of the lowest unoccupied molecular orbital (LUMO) of the neutral lumiflavin, which becomes occupied with the extra electron in the anionic state, with the changes in the bond lengths. The LUMO of the neutral lumiflavin, shown in the bottom left panel of Figure 3, shows that the extra electron is delocalized over the entire molecule. It has an antibonding character at bonds where the LUMO changes color (i.e., sign) and a bonding character at other bonds that are spanned by a high amplitude region of the one-electron wave function. Comparing the middle and bottom panels, we see that there is a strong correlation between the location of a node (zero-amplitude) or high-amplitude region of the LUMO and a shortening or elongation of the bond at that location. The exceptions to this "rule" are indicated by a red arrow in the middle panels of Figure 3, which indicate that it is somewhat too simple to regard only the shape of the LUMO.

An important ingredient in Marcus' theory of electron transfer is the assumption that the response of a polar environment behaves in a linear fashion to a transfer of charge. We can test this hypothesis also for the inner sphere reorganization. We perform this test in two ways. In the first manner, we compute the vertical energy gap, ΔE, for a series of 10 lumiflavin structures that we construct by taking a linear interpolation of the neutral and anionic geometries. Second, we optimize the lumiflavin geometry using a coupled mixture of the Hamiltonians of the neutral and charged lumiflavin as described in the Methods section (see eq 18), also for a series of 10 different coupling parameters. Comparing the results, we find that the latter optimizations with the mixed Hamiltonians result in the same geometries as the ones constructed by hand in the first series. Moreover, ΔE indeed appears in both cases as a linear function of the geometry, as shown by the lower line in Figure 4. Given the relatively small changes of the bond lengths,

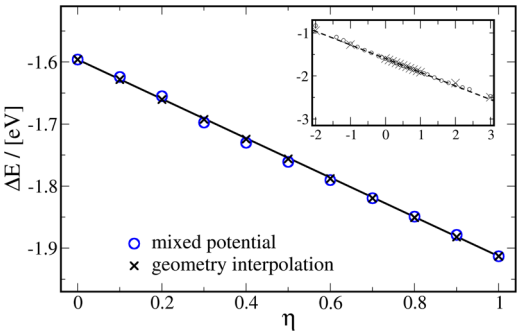

Figure 4. The vertical energy gap, ΔE, of the half reaction LF + e^- → LF^- in a vacuum as a function of the coupling parameter, η at $T = 0$ K. Taking a linear interpolation of the neutral ($\eta = 0$) and anionic ($\eta = 1$) lumiflavin geometries (× symbols) gives the same result as using a linear mixture of the Hamiltonians (○ symbols). The inset shows the remarkable linear behavior for an extended (unphysical) η range.

which are well within the amplitudes of the harmonic fluctuations at room temperature, the linear response may not come as a surprise for the shown regime of the coupling parameters from zero (neutral flavin) to one (fully charged anionic flavin). Note, however, that the inset in Figure 4 shows our calculations of ΔE in which the coupling parameter was varied from −2 to 3. It is surprising that even at these nonphysical extremes of the coupling parameter the response is still linear to a very high degree.

Lumiflavin in Water, the Solvent Structure. We performed AIMD simulations of the following four systems of aqueous lumiflavin: (1) oxidized lumiflavin (LF); (2) the reduced, anionic radical state of lumiflavin (LF^-); (3) the protonated semiquinone lumiflavin (LFH); and (4) the fully reduced lumiflavin (LFH^-). The simulations were done at T = 300 K and T = 350 K. Figure 5 shows a snapshot from the simulation of LF at T = 300 K containing the flavin molecule and the 102 water molecules in the unit cell. The figure also shows the LUMO of LF, which resembles, as expected, to a very high degree the LUMO of LF in the gas phase.

The lumiflavin molecule is an amphiphilic molecule. On one side it contains a hydrophobic carbon-ring with methyl side groups, whereas at the other end it is heterocyclic with nitrogen atoms and carbonyl groups that can form hydrogen bonds with water solvent molecules. The hydrophobic and hydrophilic parts of the molecule affect the solvent structure in different manners, which is clearly visible in snapshots taken from the AIMD simulations and can be quantified by computing the pair-correlation between lumiflavin atoms and solvent atoms. Figure 6 shows representative snapshots of the first

dx.doi.org/10.1021/ct400088g | J. Chem. Theory Comput. 2013, 9, 3889−3899

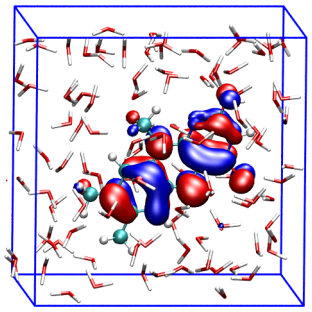

Figure 5. Snapshot of the cubic supercell containing the neutral lumiflavin in water solvent. Also shown is the lowest unoccupied molecular orbital, which is, as expected, almost identical to that in the gas phase.

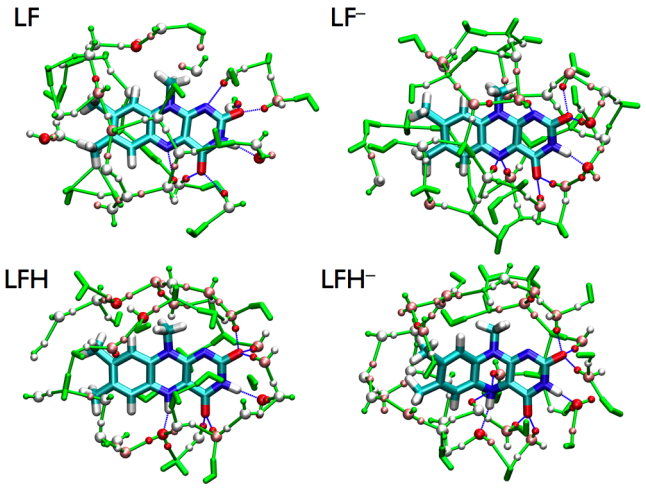

Figure 6. Representative snapshots of the first coordination shells of neutral lumiflavin (top left), anionic lumiflavin (top right), neutral semiquinone (bottom left), and doubly reduced flavin (bottom right) at T = 350 K. Water O and H atoms are colored red, pink, white, or green when within a distance to lumiflavin of respectively 2.5, 3.0, 3.5, or 4.0 Å. Thin green lines between water O and H atoms that are within 2.5 Å of each other are drawn to emphasize the water network structure. Blue lines indicate the H bonds between lumiflavin and water molecules.

coordination shell of lumiflavin in each of the four simulated neutral and anionic states. We have computed the radial distribution functions for each of the lumiflavin atoms with respect to the solvent oxygens and hydrogens. The distribution functions that show the largest changes upon changing the flavin oxidation state are shown in Figure 7.

We will first consider the radial distribution around the neutral LF and compare it with that of the reduced LF^- species, both shown in the left panels of Figure 7. Starting at the top panel, we see that the distribution function of the N1 atom with respect to the water hydrogens, H_w, shows a peak at about 1.8 Å, for both the neutral flavin (black line) and the anionic flavin (red line). Similar peaks are seen in the graphs for the O2, H3, and O4 atoms, which indicate that these atoms interact strongly with the water molecules in the first coordination shell by either donating a hydrogen bond to a water oxygen (H3 atom) or accepting a hydrogen bond from water (N1, O2, and O4 atoms). The graph of the N5 atom in the bottom panel only shows a peak in the anionic case. For the N10 nitrogen and all other carbon and hydrogen atoms, not much structure is seen in the radial distribution (data available in the Supporting

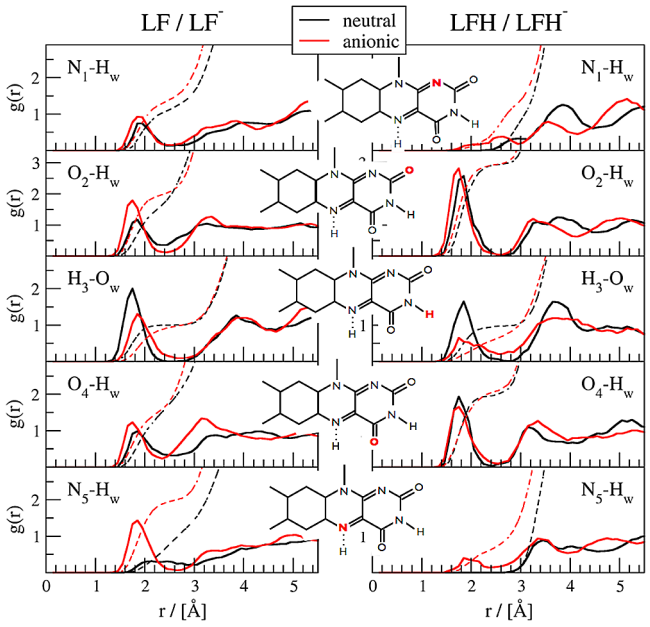

Figure 7. Radial distribution of solvent water around selected atoms of lumiflavin at T = 350 K. Left panels: neutral lumiflavin (black lines) and reduced anionic lumiflavin (red). Right panels: neutral semiquinone state, LFH (black), and doubly reduced anionic flavin, LFH^- (red). The dotted lines show the integrals from which the coordination numbers can be read.

Information), which confirms that these atoms are not involved in hydrogen bond interactions with the solvent.

The dashed lines show the normalized integrals of the distribution functions from which a quantitative estimate of the coordination can be obtained. The coordination number of each lumiflavin atom with respect to the water atoms is obtained by taking the integral over the first peak up to a limit in the next minimum, which here we set to r^{max} = 2.4 Å. The coordination numbers are compiled in Table 2. The integral

Table 2. Coordination Numbers of Selected Lumiflavin Atoms by Water Atoms, Obtained by Taking the Integral of the Radial Distribution Function over the First Peak up to r^{max} = 2.4 Å

	LF	LF^-	LFH	LFH^-
N_1-H_w	1.1	1.3	0.0	0.4
O_2-H_w	1.7	2.0	2.9	2.9
H_3-O_w	1.0	0.9	0.9	0.6
O_4-H_w	1.6	1.7	2.0	2.0
N_5-H_w	0.6	1.9	0.0	0.6

over the first peak in the $N1-H_w$ graph reveals that N1 accepts one H bond from a nearby water molecule. The O2 oxygen accepts on average 1.7 hydrogen bonds. H3 is donated to form an H bond with a water oxygen, and the O4 atom accepts on average 1.6 H bonds. This pattern of hydrogen bonds between the hydrophilic part of the neutral lumiflavin and the closest water molecules is illustrated in the top-left panel in Figure 6 by the blue lines. Although also at the hydrophobic side of LF several close water molecules (colored red) are seen, these solvent molecules are much more mobile than the molecules that form H bonds with LF and therefore do not appear as peaks in the radial distribution functions of the nearby LF atoms.

dx.doi.org/10.1021/ct400088g | J. Chem. Theory Comput. 2013, 9, 3889−3899

Comparing the neutral LF radial distribution with that of the anionic LF^-, an increase of the peak (and the coordination) of the O2−H_w curve in the second panel on the left is observed, which indicates a somewhat stronger attraction toward water molecules of this oxygen in the anionic case. In the panel below, we see the opposite effect for the H3 atom. However, the main change upon the addition of an electron to neutral LF occurs at the N5 nitrogen atom. In the neutral state only a very small and broad peak is seen in the radial distribution function that integrates to an average 0.6 H bond. In the anionic state, the N5−H graph shows a distinct peak indicating that N5 accepts two H bonds. Clearly, the N5 atom behaves rather differently toward the solvent than the N1 nitrogen. Note also that the minima at $r \approx 2.4$ Å in the distribution curves of O4 and N5 are rather shallow and not approaching zero, especially in the neutral case. This indicates that the H bonds are not very strong and that the coordinating water molecules at these sites are easily replaced by other water molecules.

It may be surprising at first that the N5 nitrogen of the neutral flavin is a much weaker acceptor of H bonds than the N1 site; however, this behavior is in agreement with the recent DFT calculations of North et al., who found that the N5 atom of lumiflavin (in gas phase) is much more electrophilic than the N1 atom.[10] Also the significant increase of the coordination of the N5 after adding an electron is in agreement with the known increase in pK_a of the flavin upon reduction, which is indeed expected to become easily protonated at the N5 position to form the neutral semiquinone state.

Next, we examine the solvent structures in the neutral semiquinone state and in the fully reduced anionic state of lumiflavin, both shown in the bottom panels of Figure 6 and represented by the radial distribution functions on the right-hand side panels of Figure 7. First, we note that the coordination shell of the LFH state shows a number of differences with respect to that of the unprotonated LF^- state, as seen from the radial distribution functions. In particular, the absence of the peak in the N1−H_w radial distribution function shows that the N1 nitrogen atom is no longer an acceptor for H bonds after protonation at the N5 atom. Second, the O2−H_w peak is more pronounced, and the average coordination number has increased from 2 to 3. Similarly, the O4−H_w peak in the distribution function shows an increase. Finally, we see that the N5 nitrogen is no longer an acceptor for H bonds after it is protonated.

Upon further reduction of the semiquinone LFH, the changes in the solvent coordination shell are smaller than those seen in the first one-electron reduction step of LF. We only note a decrease in the H3−O_w peak upon reduction, similar to, but somewhat more pronounced than in, the LF/LF^- case. At the N5 position, a very small and broad peak appears in the anionic LFH^- state, indicating that this nitrogen not only donates an H-bond but is also a weak H-bond acceptor. The snapshot shown in the bottom-right panel of Figure 6 shows two nearby solvent molecules interacting with N5; however visual inspection of the trajectory reveals that these nearby water molecules are very mobile and continuously switch these H bonds between different water molecules, the N5 nitrogen atom, or point with a hydrogen toward the center of one of the flavin rings. A striking difference of the solvation shell of the anionic LFH^- from that of LF^- is that in LF^- we saw that the N5 nitrogen is a strong H-bond acceptor, which reflects its increased proton affinity in the semiquinone state, while instead in LFH^-, the N1 site does not accept H bonds, even though it is expected to have a high proton affinity in the fully reduced state.

In the simulation of the fully reduced LFH^- state, the three-ring structure is seen to bend more than in the oxidized and semiquinone states (see, e.g., the snapshots in Figure 6). In Figure 8, we show the so-called butterfly bending of the isoalloxazine ring system (top panel), which is defined here as the average of the angles between atoms C9−N10−N1 and of C6−N5−C4. We also measured the torsion of the ring system, defined through the torsion angle spanned by atoms C6−C9−N1−C4, which is plotted in the bottom panel. The LFH^- system shows indeed much larger bending angles than the other states. The torsion angle distributions show fluctuations around average values that are somewhat shifted between the different states. Only in LF^- is the average torsion zero degrees, which is the value for the planar ring system. The butterfly bending of the ring system is known to correlate with the electron affinity of the flavin, and hereafter we will see what the role of the bending is on redox properties of lumiflavin in water.

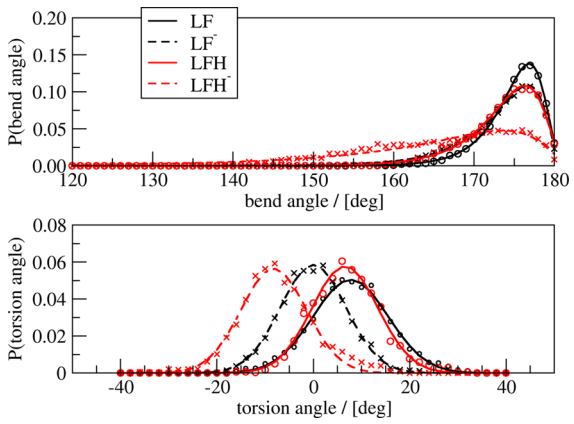

Figure 8. Bending (top panel) and torsion (bottom panel) angles of aqueous lumiflavin in different oxidation states at $T = 350$ K. The lines are curve fits to the histogram data shown as crosses and circles. The fully reduced flavin shows significant bending, while at higher oxidation states the ring structure remains planar.

Lumiflavin in Water, Redox Properties. Next, we examine the redox properties of lumiflavin in water by computing the free energy curves for the first and second one-electron reduction reactions. In practice, these reduction reactions (see eqs 1 and 3) are coupled, and second, the intermediate semiquinone radical species is known to be rather unstable. The measured reduction potentials vary strongly with the pH as the one-electron redox reactions are also coupled to the protonation reactions. The pK_a's of the oxidized, semiquinone, and fully reduced redox states of the flavin have been estimated to be 10.3, 8.5, and 6.72, respectively.[6] However, in our computer simulations, we can study the reduction reactions independent from each other and at a fixed protonation state of the flavin. We compute the free energy curves for the two reduction reactions by making a histogram of the vertical energy gap, ΔE, during an DFT−MD simulation, as explained in the Computational Setup section.

The top panels in Figure 9 show the normalized histograms of ΔE obtained from simulations in the neutral state and in the reduced anionic state for the first reduction reaction (left panels) and the second reduction (right panel). The simulations were done at $T = 300$ K (black dots in Figure 9)

dx.doi.org/10.1021/ct400088g | J. Chem. Theory Comput. 2013, 9, 3889−3899

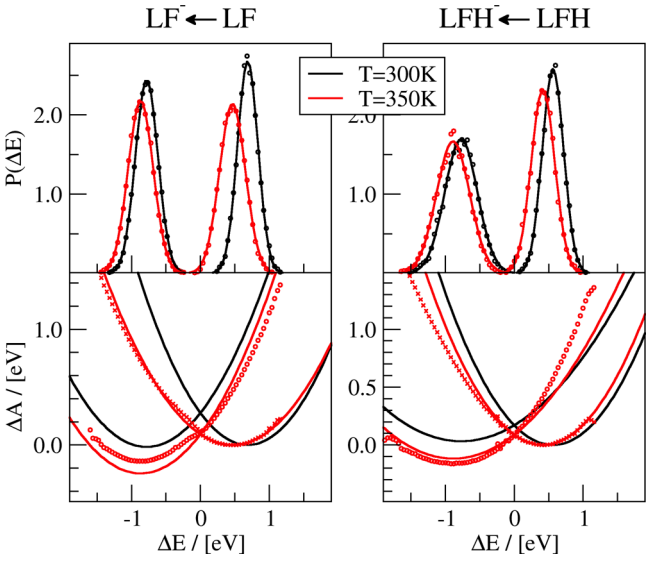

Figure 9. Top panels: distributions of the vertical energy gaps at T = 300 K (black) and T = 350 K (red) for the first flavin reduction (left panel) and second reduction (right). The solid lines are Gaussian fits of the $P(\Delta E)$ histogram from the simulation data, shown by dots. Bottom panels: free energy curves obtained from the Gaussian fits (solid lines) and the raw data (circles and crosses) using eq 8.

and T = 350 K (red dots). ΔE is in all cases found to be normally distributed, in agreement with Marcus' theory, and shows a good fit with Gaussian functions (solid lines in Figure 9). From the Gaussian fit functions we obtain the values for $\langle \Delta E \rangle_\eta$ and σ_η (see also eq 15), which are compiled in the first four rows of Table 3. The free energy curves shown in the bottom panels are obtained from the ΔE distributions in the top panels using eq 8. For the solid curves, the Gaussian fits of $P(\Delta E)$ were used, while the spheres and crosses are obtained from the dots in the top panels (only shown for T = 350 K). For the latter, we constructed the A_O curve (crosses) from the $P_O(\Delta E)$ and $P_R(\Delta E)$ distributions using the weighted histogram analysis method[38] and obtain the A_R curve (circles) by applying eq 10.

In vitro, the first and second reduction reactions are coupled, and the semiquinone states, LF^- and LFH, are rather unstable intermediates in the total reduction process. By considering the following combination of the two half-reactions:

$$LF + LFH^- \rightleftharpoons LF^- + LFH \tag{20}$$

we can estimate the semiquinone formation constant:

$$K = \frac{[LF^-][LFH]}{[LF][LFH^-]} = \exp[-\beta(\Delta A^{LF/LF^-} - \Delta A^{LFH/LFH^-})] \tag{21}$$

Filling out our $\Delta A'$ estimates at T = 350 K, $\Delta A^{LF/LF-} = -0.14$ eV and $\Delta A^{LFH/LFH-} = -0.17$ eV, gives a too large value of K = 0.37. Experimental estimates[8] of the semiquinone formation constant vary between 7.3×10^{-2} and 2.2×10^{-4}. We think that this difference may be due the PBE density functional, for which we have indications that it underestimates the electron affinity of LFH by 0.11 eV (see also Table 1). Correcting $A^{LFH/LFH-}$ gives a semiquinone formation constant of $K = 3 \times 10^{-3}$.

Nonlinearity, Inner Sphere Fluctuations, Temperature, and Finite Size Effects. In the case that the system (solute plus solvent) response is linear with respect to a change in charge, we can apply Marcus' theory of electron transfer, which implies the well-known relations for the total reaction free energy, ΔA, and the reorganization free energy, λ, that we derived in the Methods section. These relations either use the first and second moments of the ΔE distribution in the oxidized state (giving ΔA_O and λ_O) and in the reduced state (ΔA_R and λ_R) or they combine the first moments of both oxidized and reduced distributions (ΔA and λ without subscript). However, the results compiled in Table 3 show discrepancies between λ_R, λ_O, and λ and between ΔA_R, ΔA_O, and ΔA that could be an indication of nonlinear effects.

Taking a closer look at the results for the first reduction reaction, we note that the $P_O(\Delta E)$ and $P_R(\Delta E)$ distributions are well-fitted by Gaussian functions (see Figure 9) with rather similar second moments, σ_O and σ_R, as expected from Marcus' linear response theory. As a result, the values of λ_O and λ_R, which are computed from these measures of the fluctuations using eq 16, are in reasonable agreement. However both λ_O and λ_R are smaller than λ. The latter is computed from the first moments using eq 14 and is expected to converge faster with simulation length than λ_O and λ_R. The discrepancy is therefore more likely due to statistical errors that lead to an underestimation of the fluctuations than due to nonlinear effects. The underestimation of the fluctuations is also the main cause of the discrepancy between ΔA_O and ΔA_R, as they depend on λ_O and λ_R with opposite sign (see eq 16). The value for ΔA computed

Table 3. (Rows 1−4) First and Second Moments of the Vertical Energy Gap Distributions Obtained from the Gaussian Fit Functions (See Figure 9), with in Parentheses an Error Estimate in the Last Two Digits (see text) and (Rows 5−11) Redox Properties Derived from the ΔE Distributions Using the Equations Listed in the Last Column

	LF → LF⁻		LFH → LFH⁻		
T/K	300	350	300	350	equation
$\langle \Delta E \rangle_O$	0.69 (01)	0.47 (02)	0.56 (02)	0.42 (02)	15
$\langle \Delta E \rangle_R$	−0.78 (02)	−0.87 (03)	−0.77 (05)	−0.89 (04)	15
σ_O	0.15 (00)	0.19 (00)	0.15 (00)	0.17 (01)	15
σ_R	0.16 (00)	0.18 (01)	0.24 (02)	0.24 (01)	15
λ_O	0.43	0.59	0.46	0.49	16
λ_R	0.52	0.55	1.08	0.95	16
λ	0.73	0.67	0.67	0.65	14
ΔA_O	0.26	−0.12	−0.10	0.07	17
ΔA_R	−0.26	−0.31	0.31	0.06	17
ΔA	−0.05	−0.20	−0.11	−0.24	13
$\Delta A'$	0.00	−0.14	0.01	−0.17	8, 10

from only the first moments (eq 13) is in fair agreement with $\Delta A'$, which is the reaction free energy obtained from our graphs using eq 8 and without implying Gaussian statistics and linear response.

For the second reduction reaction, the situation is different. The ΔE fluctuations in the oxidized state and the corresponding value for λ_O are very similar to the numbers found for the first reduction reaction. However, in the LFH^- state, the fluctuations are significantly larger, resulting in a twice as large estimate for λ_R. In a previous section, we already noted the larger fluctuations in the butterfly bending of the flavin ring system in the fully reduced LFH^- state compared to that in the other states (see Figure 8). In Figure 10, we compare the LFH^-

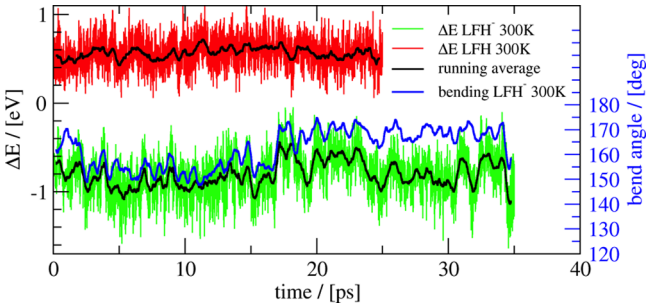

Figure 10. Comparison of the ΔE fluctuations from the simulation of the semiquinone LFH state (red line) and the reduced LFH^- state (green) at T = 300 K. A running average over 1000 MD steps (black line) is compared with the butterfly bending angle in LFH^- (blue line, RHS axis).

bending with the fluctuations in ΔE by plotting a running average with a window size of 0.5 ps. The fluctuations in ΔE are naturally due to the sum of the finite temperature motions of the vibrating lumiflavin atoms (inner shell) and that of the atoms of the polar solvent molecules (outer shell). Nevertheless, the butterfly bending shows a noticeable correlation with the fluctuations in ΔE that is prominent despite the noise due to the motions of all other collective variables. The ΔE fluctuations in the neutral LFH, the structure of which remains largely flat throughout the simulation, are indeed significantly smaller, as illustrated by the red line in Figure 10. Clearly, the increased butterfly motion in the fully reduced state induces a remarkable nonlinear contribution to the free energy landscape. We note that a similar effect has been observed for the thianthrene molecule, which is a sulfur-containing three-ring system that shows a significant butterfly bending in the neutral reduced state but becomes planar upon oxidation to a dicationic aromatic state.[20] Also in that case, the reduced thianthrene displays significantly larger energy gap fluctuations, which suggests that the observed deviation from linear response could be a generic feature for the redox properties of polycyclic molecules that switch between aromatic and nonaromatic states.

From Figure 9 we see that the effect of increasing the temperature from T = 300 to 350 K is that the $P(\Delta E)$ distributions shift to the left, that is, toward more negative ΔE values. Moreover, the $P_O(\Delta E)$ of the neutral state shifts somewhat more than the $P_R(\Delta E)$ of the anionic state. This trend can be understood by realizing that the lumiflavin will have a somewhat stronger interaction with the solvent in the anionic state compared to that in the neutral state (note for example the increased structure in the radial distribution functions for most flavin atoms). Increasing the temperature is therefore expected to induce larger fluctuations, away from the energetically most favorable solvent structure, in the neutral state than in the anionic state. As a result, E_O increases on average more than E_R, which results in a shift to more negative ΔE. From eq 13 it is clear that this shift with increasing temperature leads to a more negative reaction free energy, whereas eq 14 predicts that the larger effect on E_O compared to that on E_R will make the reorganization free energy less negative with increasing temperature. These trends are confirmed by the numbers in Table 3, except for λ_O and λ_R. The increase of the latter with temperature confirms once more that the fluctuations are underestimated due to the limited statistical sampling, which we indeed expect to improve with increasing temperature.

To estimate the statistical error in our measurements of the first and second moments of the energy gap distribution, i.e., in $\langle \Delta E \rangle$ and σ, we performed a block averaging analysis in which the trajectory is divided in M equal-sized blocks, and for each block, $\langle \Delta E \rangle$ and σ are computed. The error is taken from a plot of $\sigma_M/(M)^{1/2}$ versus the block size, with σ_M the standard deviation in $\langle \Delta E \rangle$ or σ over the M block estimates. These plots are found in the Supporting Information, and the error estimates are given in parentheses in Table 3. The statistical error analysis of $\langle \Delta E \rangle$ shows that even with a block length of 4 ps the error estimate is not converged, indicating long time correlations in ΔE. Taking the maximum value of all plots we estimate the statistical error in $\langle \Delta E \rangle$ to be 0.05 eV. Surprisingly, the same analysis on our estimate of the fluctuations gives statistical errors that are in most cases 4 or 5 times smaller. As we would expect the error in σ to be equal or larger than the error in the first moment, this leads us to conclude that even on our 20- to 40-ps-long DFT−MD simulations only the relatively fast decorrelating fluctuations are captured rather well, whereas the contributions from slower variations would require much longer sampling times.

Other, systematic errors that affect our calculations are the quality of the electronic structure calculation using the DFT−PBE/DZVP level of theory already discussed in the previous section and the finite size of the molecular system subject to periodic boundary conditions. In a recent work by Adriaanse et al., it was found that nonlinearities can arise for solutes with very negative or very positive reduction potentials with respect to the standard hydrogen electrode (SHE).[41] Apparently, the conduction band minimum of liquid water limits the vertical attachment level of poorly oxidizing species such as CO_2, whereas at the other end of the spectrum, the valence band maximum of the solvent limits the ionization potential of very strong oxidants such as the OH* and Cl* radicals. Moreover, the latter effect was found to be spuriously exaggerated by pure DFT GGA functionals. The found deviation from linearity, quantified by the asymmetry in the reorganization free energies (its ratio, λ_R/λ_O, equal to one meaning perfectly linear), is approximately proportional to the redox potential and close to absent at slightly negative potentials, such as that of O_2. The experimental first and second reduction potentials of flavin are −0.101 and −0.313 V (values for FMN taken from ref 8), which is in the regime where these nonlinearity effects due to the electronic band structure of water are expected to be minimal.

For our comparison of the first and second reduction reactions of lumiflavin, we expect that the finite size errors largely cancel, due to the similar solvent reorganization and

same box size. However, for an absolute estimate of the redox potential and the reorganization free energy a correction with respect to the infinite box size limit should be computed. Although in principle such a correction can be estimated using continuum theory or classical molecular dynamics simulations,[26,27,39,40] this goes beyond the scope of the current work. Alternatively, the offset due to the periodicity of the unit cell can in principle be eliminated by computing the SHE under the same periodic boundary conditions, in order to compare with experimental redox potentials.[21,41]

CONCLUSIONS

We have studied the first and second reduction reactions of lumiflavin in water solution at T = 300 K and T = 350 K, using Born−Oppenheimer molecular dynamics simulations at the DFT−PBE level of theory. Upon reduction of the oxidized flavin to the anionic semiquinone, the solvent structure undergoes a number of changes, in particular at the hydrophilic side of the isoalloxazine ring system. The computed radial distribution functions show that the hydrogen bonding between the lumiflavin and the coordinating water molecules becomes stronger in the anionic state, and especially the N5 nitrogen changes from a weak H-bond acceptor to a strong acceptor of two water molecules. The solvent reorganization in the second reduction reaction from the hydrated semiquinone to the fully reduced anionic lumiflavin are smaller. The carbonyl oxygens become very strong H-bond acceptors for up to three water molecules, while the N1 nitrogen remains rather inert to H bonds, unlike the N5 during the first reduction, even though it is expected to become easily protonated in the reduced state. In the fully reduced state the lumiflavin shows an increased butterfly bending, whereas in the oxidized and semiquinone states it remains largely planar. We computed the redox properties using the free energy perturbation approach for half reactions pioneered by Warshel and more recently for DFT-based molecular dynamics by Sprik et al. From the reaction free energies of the first and second reduction reactions, we can estimate the formation constant of the intermediate semiquinone radical state. The value of $K = 3 \times 10^{-3}$, after correcting for the underestimation of the electron affinity of the singly reduced flavin by the PBE density functional, is in fair agreement with experimental estimates. Comparing the reduction free energies with the values obtained using the well-known relations obtained from Marcus theory reveals discrepancies that could indicate that nonlinear effects in the solvent response play a role. Indeed, for the second reduction reaction a significant increase in the energy gap fluctuations in the fully reduced state shows that in that case Marcus' linear response approximation does not hold. A prominent correlation between the energy gap fluctuations and the butterfly bend angle indicates that this inner sphere reorganization and its coupling to the solvent is the cause of the nonlinearity. A second source of discrepancy is the systematic underestimation of the energy gap fluctuations. The spurious increase of the reorganization free energy with temperature when computed from the energy gap fluctuations as well as our analysis of the statistical errors using block averages indicate that much longer sampling times are needed to converge an estimate of the energy gap fluctuations.

ASSOCIATED CONTENT

Supporting Information

A graph showing the basis set dependence of the lumiflavin electron affinity, structural motif and labeling of lumiflavin, additional radial distribution functions of solvent water around lumiflavin, the raw gap energy data, and block averaging based error analysis. This information is available free of charge via the Internet at http://pubs.acs.org

AUTHOR INFORMATION

Corresponding Author

*E-mail: B.Ensing@uva.nl.

Notes

The authors declare no competing financial interest.

ACKNOWLEDGMENTS

The work was financially supported by NWO (The Netherlands Organization for Scientific Research) through a Vidi grant of B.E.

REFERENCES

(1) Ghisla, S.; Massey, V. *Eur. J. Biochem.* **1989**, *181*, 1−17.
(2) Walsh, J.; Miller, A. *J. Mol. Struct. (THEOCHEM)* **2003**, *623*, 185−195.
(3) Arents, J. C.; Perez, M. A.; Hendriks, J.; Hellingwerf, K. J. *FEBS Lett.* **2011**, *585*, 167−72.
(4) Mathes, T.; van Stokkum, I. H. M.; Stierl, M.; Kennis, J. T. M. *J. Biol. Chem.* **2012**, *287*, 31725−38.
(5) Hasford, J. J.; Rizzo, C. J. *J. Am. Chem. Soc.* **1998**, *120*, 2251−2255.
(6) Draper, R.; Ingraham, L. L. *Arch. Biochem. Biophys.* **1969**, *125*, 802−808.
(7) Anderson, R. *Biochim. Biophys. Acta* **1983**, *722*, 158−162.
(8) Mayhew, S. G. *Eur. J. Biochem.* **1999**, *265*, 698−702.
(9) Bhattacharyya, S.; Stankovich, M.; Truhlar, D. G.; Gao, J. *J. Phys. Chem. A* **2007**, *111*, 5729−42.
(10) North, M.; Bhattacharyya, S.; Truhlar, D. G. *J. Phys. Chem. B* **2010**, *114*, 14907−15.
(11) Zeng, X.; Hu, H.; Hu, X.; Yang, W. *J. Chem. Phys.* **2009**, *130*, 164111.
(12) Warshel, A. *J. Phys. Chem.* **1982**, *86*, 2218−2224.
(13) King, G.; Warshel, A. *J. Chem. Phys.* **1990**, *93*, 8682.
(14) Blumberger, J.; Bernasconi, L.; Tavernelli, I.; Vuilleumier, R.; Sprik, M. *J. Am. Chem. Soc.* **2004**, *126*, 3928−38.
(15) Blumberger, J.; Sprik, M. *J. Phys. Chem. B* **2004**, *108*, 6529−6535.
(16) Blumberger, J.; Tavernelli, I.; Klein, M. L.; Sprik, M. *J. Chem. Phys.* **2006**, *124*, 64507.
(17) Blumberger, J.; Sprik, M. *J. Phys. Chem. B* **2005**, *109*, 6793−804.
(18) Blumberger, J.; Sprik, M. *Theor. Chem. Acc.* **2005**, *115*, 113−126.
(19) VandeVondele, J.; Sulpizi, M.; Sprik, M. *Angew. Chem., Int. Ed.* **2006**, *45*, 1936−38.
(20) VandeVondele, J.; Lynden-Bell, R.; Meijer, E. J.; Sprik, M. *J. Phys. Chem. B* **2006**, *110*, 3614−23.
(21) Costanzo, F.; Sulpizi, M.; Della Valle, R. G.; Sprik, M. *J. Chem. Phys.* **2011**, *134*, 244508.
(22) Blumberger, J. *J. Am. Chem. Soc.* **2008**, *130*, 16065−68.
(23) Vuilleumier, R.; Tay, K. A.; Jeanmairet, G.; Borgis, D.; Boutin, A. *J. Am. Chem. Soc.* **2011**, *134*, 2067−74.
(24) Marcus, R. *J. Chem. Phys.* **1956**, *24*, 979.
(25) Marcus, R. *Rev. Mod. Phys.* **1993**, *65*, 599−610.
(26) Hummer, G.; Pratt, L. R.; Garcia, A. E. *J. Phys. Chem.* **1997**, *100*, 1206−1215.
(27) Cheng, J.; Sulpizi, M.; Sprik, M. *J. Chem. Phys.* **2009**, *131*, 154504.

(28) Perdew, J.; Burke, K.; Ernzerhof, M. *Phys. Rev. Lett.* **1996**, *77*, 3865−3868.
(29) VandeVondele, J.; Krack, M.; Mohamed, F.; Parrinello, M.; Chassaing, T.; Hutter, J. *Comput. Phys. Commun.* **2005**, *167*, 103−128.
(30) CP2K developers group. http://cp2k.berlios.de.
(31) Lippert, G.; Hutter, J.; Parrinello, M. *Mol. Phys.* **1997**, *92*, 477−487.
(32) Goedecker, S.; Teter, M.; Hutter, J. *Phys. Rev. B* **1996**, *54*, 1703.
(33) Hartwigsen, C.; Godecker, S.; Hutter, J. *Phys. Rev. B* **1998**, *58*, 3641.
(34) VandeVondele, J.; Hutter, J. *J. Chem. Phys.* **2007**, *127*, 114105.
(35) Martyna, G. J.; Tuckerman, M. E. *J. Chem. Phys.* **1999**, *110*, 2810.
(36) Bussi, G.; Donadio, D.; Parrinello, M. *J. Phys. Chem. A* **2007**, *126*, 014101.
(37) Kuo, I. F. W.; Mundy, C. J.; McGrath, M. J.; Siepmann, J. I. *J. Chem. Theory Comput.* **2006**, *2*, 1274−1281.
(38) Kumar, S.; Bouzida, D.; Swendsen, R. H.; Kollman, P. A.; Rosenberg, J. M. *J. Comput. Chem.* **1992**, *13*, 1011−21.
(39) Ayala, R.; Sprik, M. *J. Phys. Chem. B* **2008**, *112*, 257−269.
(40) Seidel, R.; Faubel, M.; Winter, B.; Blumberger, J. *J. Am. Chem. Soc.* **2009**, *131*, 16127−37.
(41) Adriaanse, C.; Cheng, J.; Chau, V.; Sulpizi, M.; VandeVondele, J.; Sprik, M. *J. Phys. Chem. Lett.* **2012**, *3*, 3411−15.

NOTE ADDED AFTER ASAP PUBLICATION

After this paper was published ASAP on August 15, 2013, a correction was made to Table 3. The corrected version was reposted August 22, 2013.